Experimental Verification of Threshold Switching in Cadmium Telluride Photovoltaics

by

Suman Devkota

Submitted in Partial Fulfillment of the Requirements

for the Degree of

Master of Science in Engineering

in

Electrical Engineering

YOUNGSTOWN STATE UNIVERSITY

May 2023

Experimental Verification of Threshold Switching in Cadmium Telluride Photovoltaics

Suman Devkota

I hereby release this thesis to the public. I understand that this **thesis** will be made available from the OhioLINK ETD Center and the Maag Library Circulation Desk for public access. I also authorize the University or other individuals to make copies of this thesis as needed for scholarly research.

Signature:

Suman Devkota, Student Date

Approvals:

Dr. Vamsi Borra, Thesis Advisor Date

Dr. Daniel Georgiev, Committee Member Date

Dr. Victor Karpov, Committee Member Date

Prof. Ghassan Salim, Committee Member Date

Dr. Salvatore A. Sanders, Dean, College of Graduate Studies Date

ABSTRACT

The use of renewable and sustainable energy sources such as solar cells have been increasing slowly and gradually. With the rapid increase and growth of solar photovoltaics (PV) production, approximately 22% from 2010 to 2020, high number of PV cells are being manufactured annually. Solar cells have been proven to be an efficient source of renewable energy because of their availability, installation, and affordability. Among all the different types of solar cells, thin-film PV has several advantages over other technologies because of its need for relatively fewer resources, ability to fully automate fabrication process, and the option to fabricate on a more affordable substrate. Nevertheless, the manufacturing process of these thin-film solar cells still involves several critical steps. For example, they still rely on conventional method of laser scribing techniques which in addition to being time consuming, has several reliability issues as well.

In this project, the theory of threshold switching method is experimentally verified on Cadmium Telluride (CdTe) PV. The study was conducted by applying different voltage bias configurations to the sample. A drastic decrease in the resistance was observed. The time lapse study of decreased resistance was conducted, which proved that the resistance change is indeed a permanent phenomenon. Our experimental results of threshold switching indicates that this could potentially lead to a scribe-less technology in manufacturing of solar cells which may potentially lead to an increase in manufacturing reliability and efficiency.

Table of Contents

List of Figures

List of Tables

List of Abbreviations

PV……Photovoltaic
CdTe…… Cadmium Telluride
CdS…… Cadmium Sulfide
Cr…… ……..……...Chromium
SEM……... Scanning Electron Microscopy
FIB……...Focal Ion Beam
TEM……..Transmission Electron Microscopy
EDS…….….Energy Dispersive Spectroscopy
AES…….…..Auger Electron Spectroscopy
ASM…….……..Auger Scanning Microscopy
TCO……....Transparent Conductive Oxide
RF……Radio Frequency

ACKNOWLEDGEMENT

I would like to take this opportunity to thank my advisor Dr. Vamsi Borra for constant, immense support, and guidance during my study and research. Dr. Borra has been always informative and supportive. I appreciate his dedication, and frequent suggestions, that he provided; which improved me as a researcher. I would also like to thank the department of Electrical and Computer Engineering for providing me with the opportunity to conduct this research and helping with all necessary funding.

I would like to express my sincere gratitude towards my collaborators Dr. Daniel Georgiev and Dr. Karpov for their constant feedback and guidance. I am glad to receive help from Drew Hirt and Material Research Lab for characterization required for this research. I would also like to thank the faculty Professor Ghassan Salim, Professor Edward Burden, and Professor Robert Caven for their support inspiration throughout all my semesters. I am grateful towards my colleagues for their support and feedback.

Lastly, I would like to thank my beloved wife for her constant dedication and support she provided throughout the journey of my master's degree. I am thankful to my parents, and entire family for their support and love they have been provided.

Chapter I

1. INTRODUCTION

1.1 Background

As we navigate the challenges of meeting our growing energy needs, it's crucial to find sustainable alternatives to non-renewable sources such as crude oils, coal, and natural gas. These sources are finite and have detrimental environmental impacts, raising concerns about their sustainability. It's imperative to invest in innovative, eco-friendly ways to power our world while preserving our resources.

With the excessive use of fossil fuels, global warming has been one of the major issues of our century. Solar energy is one of the clean and sustainable alternative sources of energy. Photovoltaic (PV) technologies have grown as one of the sustainable fields of research with thousands of publications and patents [1]. French physicist Alexandre-Edmond Becquerel discovered photovoltaic effect in 1839, which is known to be an effect that converts solar energy to electrical energy [2]. After more than a century around mid-1900's production of PV cell started in Bell laboratory which resulted in high demand for the PV industry over the world with growth rate of 40% per year [3].

There are various types of PV cells available in the market. The two major commercially available solar cell technologies are crystalline silicon technology and thin-film technology. Crystalline silicon technology comprises of monocrystalline, polycrystalline, PERC, half-cell, double glass, bifacial, GaAs and HIT modules. Abundancy of silicon on earth facilitated crystalline silicon technology to consume most of the PV market earlier. Crystalline silicon PV represented 90% of the total PV cell production in 2008 [4]. However, the life span for PV generated using this technology is nearly 20 years. PV

modules are required to supply electrical power to many applications and are assembled by interconnecting different numbers of solar cells depending upon the application [5]–[7]. Rapid failure of the interconnections has been key challenge for silicon crystalline technology as these interconnections are necessary as electrical, thermal, and mechanical contacts between the electrodes and semiconductors [2], [5], [8]. In addition to this, large production of PV has skyrocketed in term of production cost. Therefore, in recent years to overcome the challenge of silicon wafers thin-film PV is growing at a fast pace, rising to 0.6-2.7 TW_p by 2050 [3], [9].

Thin-film technology comprises of four major types: amorphous, CdTe, CIGS, and organic solar panels. The demand of thin film is high in the sustainable market because of its low production cost, semiconductor material used, easy installation, light weight, and flexibility. The production of thin-film PV may be fully automated too. The use of low semiconductor material and the flexibility of using an inexpensive foreign substrate, like low-cost soda lime glass, reduces the production cost [3], [10]. However, the production of the thin-film solar cells involves the use of expensive lasers involved to isolate the cells and create an interconnection pathway between. The types of scribing used for manufacturing of thin-film solar cells are P1, P2, and P3 patterning [11]. In order to eliminate pitfalls of commercial solar cell manufacturing, we focus on threshold switching phenomenon. This phenomenon can simply be described as a well-controlled process with a defining property of drastic decrease in resistance under electric field after a certain threshold value is exceeded. It creates a narrow conducting filament via characterization re-arrangement of structural defects, impurities, or electric dipoles. Various materials and

metal oxides have been shown to exhibit threshold switching [12]. It can be an essential building block of electronic circuits and systems.

Thus, in this study we focus on this phenomenon of threshold switching and experimentally verify it on CdTe PV which could potentially lead to scribe less technology during the manufacturing of thin-film PV resulting into reduction of the cost added using expensive laser technologies.

1.2 Motivation

Climate change is one of the major issues that the world is facing now. With the global increase in temperature by one degree Celsius over the last century [1] PV have been the best alternative source of renewable energy, among which thin film is becoming more popular in the sustainable market. Yet, manufacturing of this best alternative source is expensive.

Scribing is an extra step which is involved in manufacturing of conventional thin films. Laser scribing is used for cell isolation and to create a connecting path between contacts in PV cells. Each extra step during manufacturing can be seen as a has a potential "point of failure". Thus, reducing the steps could potentially lead to more efficient method of manufacturing PVs in terms of reliability and cost. Thus, the motivation for this study lead into the direction where manufacturing cost of thin-film PV can be reduced.

1.3 Purpose

The purpose of this thesis is to study the threshold switching phenomenon in thin-film CdTe PV and the impact in the manufacturing process by reducing the cost by eliminating

the expensive laser scribing technique. Currently, expensive laser scribing technique are used to create a conductive path during manufacturing of thin-film solar PV, while the threshold switching phenomenon creates a conductive path through solar PV to contact the buried electrode which could potentially eliminate the use of expensive laser scribing techniques used.

1.4 Objectives

The objective of this study is:

- Design an experiment to verify the threshold switching phenomenon in CdTe PV.
- Reliability study of created contact.
- Characterization of the thin-film sample.
- Study the characteristics curve of the sample across front and back contact.
- Deposit circular chromium dots to eliminate the layer of back contact.
- Experimentally verify threshold switching phenomenon on Cr dotted PV sample.

1.4 Organization

This work is divided into 5 chapters. Chapter II provides the literature review on PV, Manufacturing of thin-film, Electrical contacts, threshold switching, and characterization techniques used in the study. Chapter III represents and discusses the experimental methods carried out, chapter IV provides the results, and chapter V summarizes the content and conclude the research work.

Chapter II

2. Literature Review

2.1 Photovoltaics (PV)

Photovoltaics is the technology that converts light into electricity. PV cells are used for the conversion of light energy to electricity. When a sunlight strikes the PV cell the photons are either absorbed, transmitted, or reflected; only those photons which are absorbed provides energy to generate electricity. PV cell are made of semiconductor materials. The semiconductor part of PV cells consists of three layers, n-layer, p-layer, and depletion layer. The n-types material has access of electrons, depletion layers is the layer formed between n-type and p-type layers, the p-type layer is the layer where there is access of positively charged holes. Figure below shows the general p-n junction in PV cells.

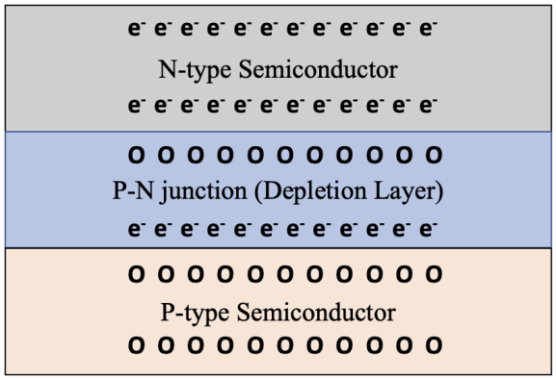

Figure 1: P-N junction in PV cell e- and o represent electrons and holes respectively.

Due to the electron migration from n type region to depletion region the boundary of n-region becomes slightly positive, and p-regions becomes slightly negative due to migration of holes in depletion region. When light strikes the PV cells it penetrates and recaches the depletion region and these light photons are sufficient to generate electron hole pairs in the

region. The electric field in the depletion region drives out the electron hole from the depletion region resulting in the increased concentration of electrons in n-region and holes in p-region which creates a potential difference between them. When an external load is connected to the n and p type region electron starts to follow towards the holes generating electric current. Figure below represents the schematic of a solar PV cell. The interconnection of these small PV cells results in producing enough electricity to operate heavy electric loads.

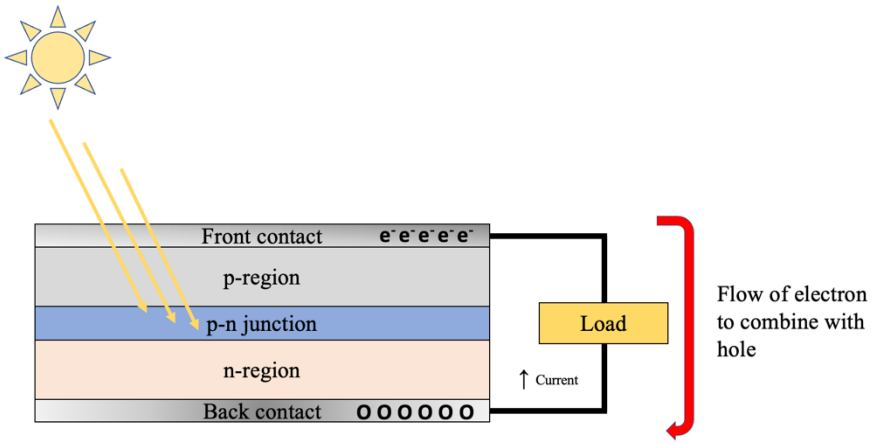

Figure 2: Schematic of Solar PV cell.

There are different types of PV technologies on the market. Among which thin film have been preferred in sustainable market because they consume relatively less semiconductor material and the fabrication process can be fully automated [3], [10]. Although there are many merits of PV technology, it has many challenges such as the desired power generation being lower than expected, lower threshold for corrosion, high chance of delamination, interconnection failure due to degradation of solder joints. This leads to a decreased life span of solar cell in addition to challenges resulting from resource availability and

environmental impact [5], [10], [13].With the increasing demand of the energy consumption worldwide, especially for electricity, it is better to develop energy saving technologies [14]. Thin-film PVs are one of the leading solar PV technologies that offers the advantages of low material consumption and mechanical flexibility [15]. Thin films technology also has the potential to produce cost effective PV-generated electronics because of its efficiency, simple installation process and lower maintenance requirements. There has been many studies done in thin film technology which led to it being commercially available in marketplace [16]. The current challenges for thin-film technology are to improve the solar cell performance for which several research on these thin films is still ongoing [17]. Among all other thin films this study here is focused on CdTe thin film PV.

CdTe has been one of the most popular types of thin film solar technology in use today. The ideal energy gap of CdTe solar cell is 1.45eV [18]. CdTe solar cell have attracted researchers' attention worldwide over decades to develop low-cost and better efficiency for PV solar energy conversion [19]. Numbers of research studies have been done to improve the efficiency and decrease the cost of manufacturing in the past and there is still ongoing research in many different laboratories worldwide. Several manufacturing techniques has been used to manufacture CdTe solar cells and those manufacturing techniques impact on the performance of the CdTe solar cell [18], [20]. Figure 3 represents the sectional structure of CdTe represents glass with SnO_2 coated on it followed by n-doped CdS with p-doped CdTe and metal for back contact.

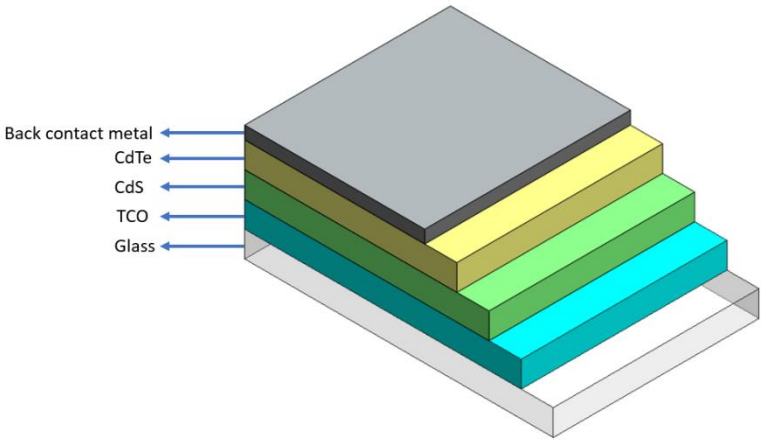

Figure 3: Cross-sectional view (not to scale) of CdTe PV.

2.2 Deposition technique

Sputtering is the process of depositing thin layer of materials onto the surface of a substrate. Sputtering technique was first reported in early 1800s and was dominating the optical coating market by 1880 [21]. With wide range of application sputtering technique has not only dominated optical market but also dominated automotive, airplane, semiconductor manufacturing industry today [21]. Using sputtering technique any material can be vaporized. Different vacuum deposition techniques like DC, RF, Magnetron, and Reactive are popular based on their application [22]. The general principle for the working mechanism of all these techniques are almost same. It is possible to produce dynamically clean surface in an inert-gas atmosphere with the base pressure of 10^{-5} torr [22]. Figure below shows the working principle of a sputtering technique where ion from the sputtering gas is used to hit the target that will result in the ejection of an atom from the target towards the substrate resulting in the deposition of thin film.

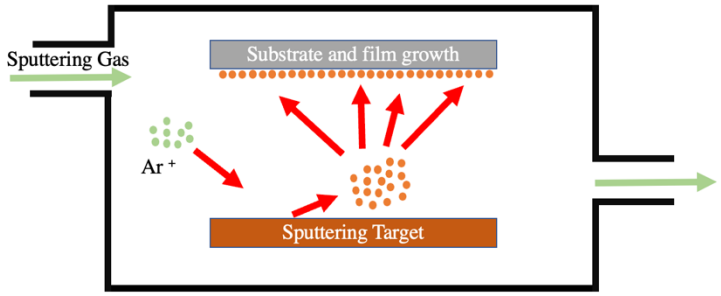

Figure 4: Working Mechanism of Sputtering deposition.

In DC sputtering the substrate is generally fixed to an anode and the material to be deposited is mounted on cathode. Sputtering gas is slowly fed into the chamber, generally inert gas is used as a sputtering gas. Pressure inside the chamber is pumped down to reach base pressure of $x10^{-7}$ micron and dc supply voltage is gradually increased until visible glow above cathode. High frequency voltage is used with sufficient amplitude that creates glow above cathode in case of RF sputtering. In technique such as RF sputtering both target and substrate may be sputtered simultaneously [22]. Magnetron sputtering is the deposition done in the presence of magnetic field where magnetic field applied forces the electron to take a certain circular path about the field's lines. The sample that has been used in this study was prepared using vapor transport deposition and RF magnetron sputtering.

2.3 Manufacturing of thin film PV

Thin films are manufactured using both vacuum and non-vacuum techniques. Different types of techniques that industry have been using are co-evaporation [23][24], physical vapor deposition [24], [25], pulsed laser deposition [24], [26], chemical vapor deposition

[24], [27], metalorganic chemical vapor deposition [24], [27], electron beam deposition [24], [28], molecular beam epitaxy [24], [29], radio frequency and dc sputtering [30]. These are all vacuum techniques that have been popular and modified to achieve cost effective approach so far. Among all these sputtering can produce large area which is suitable for industrial production [24]. Also vacuum methods are more reliable and efficient during fabrication process. During manufacturing process of thin film along with different layers of deposition laser scribing is equally used to create a pathway for electron to reach buried electrode. Different types of laser scribing techniques are used during manufacturing of the thin films, among which P3 process is the most popular [31]. The two main process under P3 process are P3 'type 1' and P3 'type 2'. Laser scribing, done to remove the layers to expose back contact, is P3 'type 1,' whereas the removal of front contact only is P3 'type 2' [31]. Figure 5 represents the schematic view of P1, P2 and P3 laser scribing process done during manufacturing of the thin film solar PV.

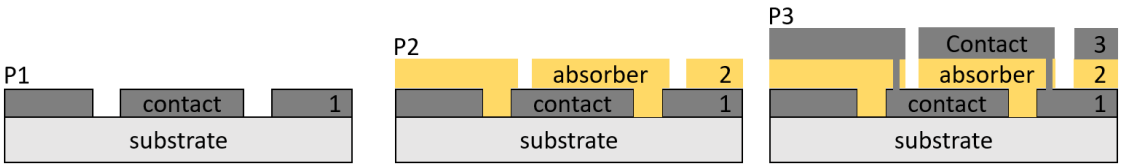

Figure 5: Isolation created to a contact using P1 scribing process (P1). Scribe done after deposition of absorber (P2). Scribe done to expose the back contact by removing front contact and absorber (P3).

After the deposition and scribing process during manufacture of thin film, the PV samples are subjected to the standard anneal in the presence of $CdCl_2$ vapor, which is done to improve the electrical characteristics of the PV manufactured [32].

The scribing techniques used by manufactures are conventional, tedious, time consuming, and expensive. This thesis presents a study of threshold switching on CdTe thin film PV

where a drastic decrease in resistance value across front and back contact implies that there is a conductive shunt created where a buried electrode can be contacted. The laser scribing techniques used in manufacturing of thin films are used to routinely contact the buried electrode as shown in Figure 5.P3 where there is a path through contact 3 to contact 1 created using a laser scribe. This conventional technique can be eliminated, saving resources, time, and lowering the manufacturing cost of the thin film solar PV.

2.4 Electrical Contact

Performance of solar PVs are important because of its wide range of applications. There are numerous factors that PV cells rely on when it comes to efficiency and performance. One of the major factors is the electrical contacts that have been used. Electrical contacts are the pathways for electrons to carry electrical current to an external load and back to a PV cell. Front contacts are used to carry electrons out of the cell, whereas back contacts are used to bring electrons back to the PV cell, completing the electrical circuit. PV cells use conducting metals as a contact. How this metal behaves in different situations determines the performance of solar cells [33], [34]. Over the years it has been known that the back contact layer is essential to increase the performance of PV, however, there is an ongoing challenge in the field regarding the most appropriate and effective metal to be used as a back contact layer. Moreover, very few studies have focused on electrical contacts, this makes it more challenging to understand and improve the performance of the solar cells. There are several elements used as a back contact among which only Au and Pd have been proven to have had a better performance. However, these elements are expensive thus, a compromise is made by replacing Au and Pd as a back contact with Mo, Ni, Sb. This

provides a relatively increased efficiency than any other element used as a back contact [33], [35]–[37].

Phenomenon of threshold switching creates the conductive pathway to the contact, the buried electrode, which will eliminate the use of back contact. Thus, this study creates a path for cost effective approach as well as decreasing the use of raw material during the manufacturing process of thin film PV.

2.5 Threshold Switching

An article published in 1968 first talked about the rapid, symmetrical, and non-destructive high-field electrical breakdown in thin films of a chalcogenide alloy amorphous semiconductor, where they announced the electric field induced threshold switching. Threshold processes for thin layers of chalcogenide glass were reported by Ovshinsky in 1968, since then there have been many attempts to explain this observation [38], [39]. Along with chalcogenide films, there are several other materials that exhibit the phenomenon of threshold switching [40].

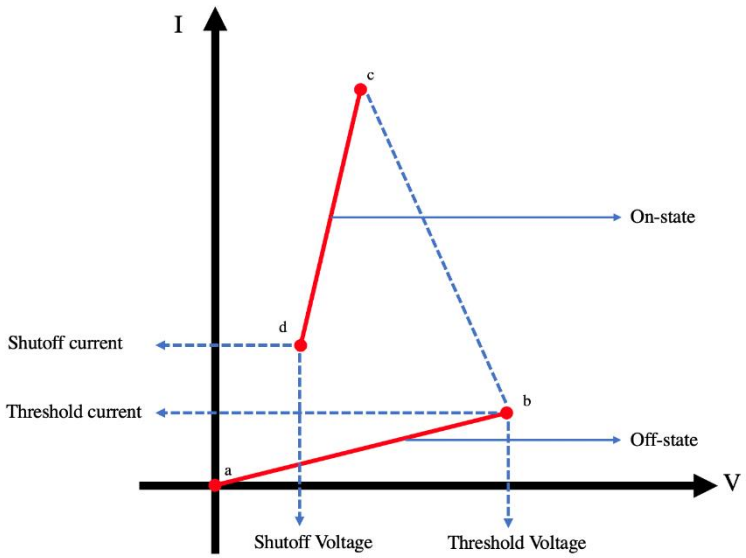

Figure 6: I-V curve for ideal threshold modulator.

Threshold switching is a well-controlled process with a defining property of a drastic decrease in resistance under electric fields exceeding a certain threshold value [40][41]. The microscopic mechanism of threshold switching varies between systems. Threshold switching takes place by creating a narrow conducting filament, either via characterization or re-arrangement of certain structural defects, impurities, or electric dipole [40][42][43]. There are many other materials that exhibit the phenomenon of threshold switching[39]. However, various metal oxides have also exhibited the phenomenon of threshold switching [40]. The dynamic response of threshold switching is an intriguing feature, for a novel building block of electrical circuits and systems [44]. Threshold switching possesses a wide range of applications like a steep subthreshold slope transistor, access devices on crossbar array, artificial synapses, and true random number generators [44].

Here, we are focused on threshold switching phenomenon in thin film CdTe PV, where switching effects are observed by recording the value of resistance before and after supplying different voltage bias-configurations.

2.6 Material characterization

Characterization of materials is the process of determining the behavior and properties of materials which include physical, mechanical, and electrical properties. It is also used to determine the microstructure, composition, and different features of samples which directly or indirectly impacts the performance based on the application. This study uses several characterization techniques like Scanning Electron Microscopy, Focal Ion Beam, Transmission Electron Microscopy, Auger Electron Spectroscopy, and Energy Dispersion Spectroscopy to determine the different features of the samples used for the experiment.

2.6.1 Scanning Electron Microscopy (SEM)

Scanning Electron Microscopy is a type of imaging technique that generates images of solid samples. SEM uses high electron beam with significant amount of kinetic energy. The energy from electrons is dissipated as different signals while interacting with the sample. Secondary and backscattered electrons are two different types of signals, which are generally used to generate an image of the sample. SEM uses secondary electrons to show morphology and topography of the sample by using secondary electrons while backscattered electrons are used to demonstrate contrast in multiphase samples. The minimum magnification for most of the SEM ranges from x20 to x50 and maximum range

may be as high as x300,000. Magnification is determined by the size of the electron beam. The spatial resolution for SEM ranges from 50nm to 100nm, however, high end SEM may have a resolution of 0.5nm. In addition to gathering imaging information to show the morphology of sample, SEM gathers X-ray beams with an energy dispersive X-ray spectrometer or EDS system, which can be used to get the information on elements of the sample. Figure 7 below demonstrates the working principle of SEM.

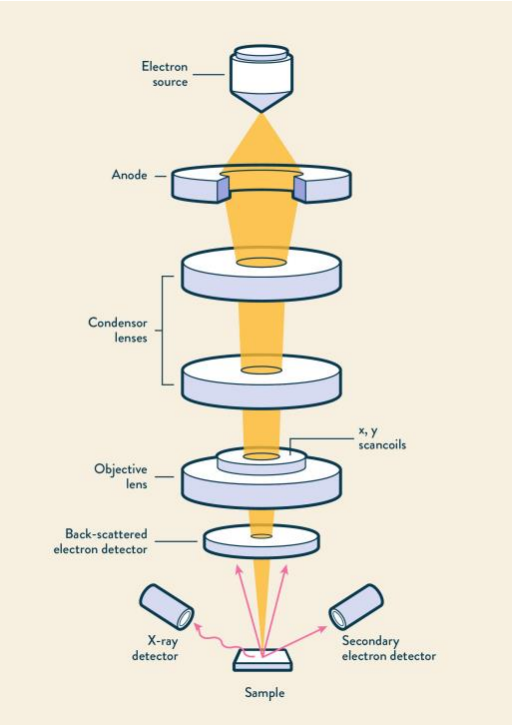

Figure 7: Closer look into SEM Working Principle [45].

Figure 7 displays the working of the SEM where the source of electrons is a tungsten filament lamp. The emission of electrons happens when thermal energy is applied to the source. The samples are mounted with thin layer of heavy metal to facilitate the scattering of charges. When the secondary electrons reach the detector, it produces the image not unlike a television, that can be viewed and captured.

2.6.2 Focused Ion Beam (FIB)

Focused Ion Beam is a technique used to remove and deposit material at nanoscale. The resolution for deposition can be less than 100nm. FIB has been excessively used as a surface patterning technique [46]. Semiconductors and chip manufacturing processes use FIB, and it's also used in SEM and TEM for sample preparation. FIB uses gallium ions that are accelerated using a strong electric field[47]. With the help of high energy-ions, FIB is used to remove material through physical sputtering. By scanning the ions, shapes and patterns may be generated on hard or brittle material. With the principle of chemical vapor deposition technique, FIB may be used to deposit material as well. Thus, FIB can be applied to both material removal and deposition techniques [47].

2.6.3 Transmission Electron Microscopy (TEM)

Transmission Electron Microscopy is the imaging technique used to generate the image of a thin specimen, through which an electron can pass. TEM uses transmission electrons to generate the images. The working principle of TEM in general is like a regular optical microscope. However, the wavelength of electrons is much smaller than light, which results in an image resolution higher than a conventional optical microscope. TEM is a very powerful imaging technique that provides various information from the sample down to atomic level. The sample on TEM should be very thin, in the range of ~200nm, which results in easy transmission of electrons to obtain a specific image, depending on the information desired, using TEM characterization [48]. Figure 8 below is the closer look into working of TEM.

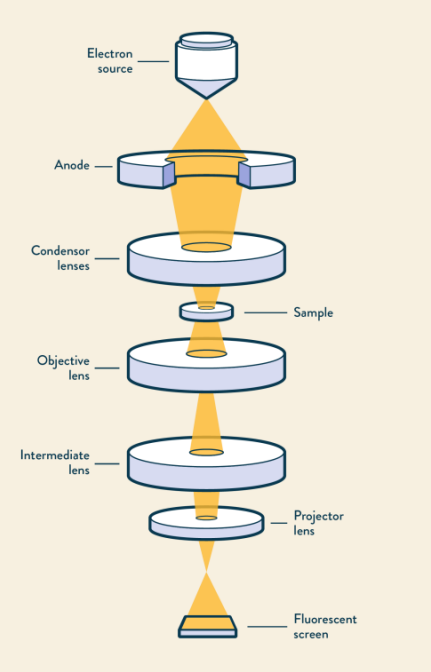

Figure 8: Closer look into TEM Working Principle [45].

2.6.4 Energy Dispersive Spectroscopy (EDS)

Energy Dispersive Spectroscopy (EDS) is a material characterization technique used to determine the elemental analysis of materials. EDS utilizes SEM and TEM to provide chemical analysis of the materials. EDS is mostly used to determine the chemical composition of the samples. When a sample is bombarded with an electron gun using high energy, some of the energies are observed, resulting from the excitation of atoms, and emitting x-ray photons from the sample. The emitted x-ray photons are detected using an energy dispersive detector which converts x-rays photons into electrical signals. The signals are then compared to a database to determine the elements present in the sample.

EDS is a widely used characterization technique; however, it comes with its own challenge. If a sample with low concentration of element is exposed to EDS there will not be enough x-rays emitting photons which will limit the capacity of identifying element. Despite its challenges EDS has been extensively used in the field of research as it provides quick elemental composition of a sample. It has been used in several fields like Material Science, Geology, Semiconductor research etc.

2.6.5 Auger Electron Spectroscopy (AES)

Auger electron spectroscopy or scanning Auger microscopy (AES/SAM) uses a focused beam of electrons to bombard a solid surface. This energetic electron beam (1-30keV and a current of 0.01-10μA) knocks out electrons from inner electron orbital shells of atoms. Electrons from outer shells can move into the inner shell vacancies as replacements for the ejected electrons. For each such atomic relaxation transition, the energy difference between the outer and inner shell electrons is released by the atom. This energy is emitted either as a characteristic x-ray or as an outer shell electron that has absorbed the energy released by the atomic relaxation process. Electrons released during relaxation of stimulated atoms are called Auger electrons (after Pierre Auger who discovered and explained the process). Those Auger electrons that are produced within the top 2-10nm (20-100Å) of the surface can escape with their full energy and result in a characteristic Auger spectrum for each element. Only H and He are excluded since they have no outer shell electrons to eject in any of their compound forms. Auger peaks are generally plotted as counts versus kinetic energy or differentiated counts versus kinetic energy. The elements present in an Auger spectrum can be readily identified by referring to a chart of 'Principal Auger Electron

Energies' that is generally available in the scientific literature. If the thin film analysis capability of AES is combined with the material removing capability of ion beam etching, then the composition variation with depth into the sample can be investigated and/or extraneous surface contamination can be removed.

CHAPTER III

3. Methods

3.1 Sample Preparation

The CdTe PV samples were prepared using two different techniques: vapor deposition and radio frequency magnetron sputtering. These two techniques have been commercially used and optimized to reduce cost. The substrate that we used to grow our PV sample is easily available SnO_2-coated glass. A layer of CdS followed by CdTe was deposited on top of TCO. The obtained samples were treated with a standard annealing process in the presence of $CdCl_2$ vapor. Annealing with the presence of $CdCl_2$ vapor results in better electrical improvements. After treating with $CdCl_2$, a thin layer of metal, in this case Cr, was deposited as a back contact material. Figure 9 shows the vacuum system where deposition of Cr had taken place in the Rf/Magnetron lab at Youngstown State University.

Figure 9: RF/Magnetron Sputtering Lab.

Before depositing any material, the substrate was treated with standard cleaning procedure. The substrate was first placed on a clean white sheet and then was washed with acetone by

dipping and rinsing it, followed by drying with blow dryer and cotton swab. Immediately after washing the substrate with acetone, the same procedure, as previously stated, was followed using IPA. For final cleaning, de-ionized water was used and only a blow dryer was used to dry the substrate. The substrate was also treated with hot plate placed inside the laboratory hood, to ensure it was dried properly. Only substrates that followed the above-mentioned procedure were used for deposition. Using the deposition techniques mentioned above, samples were created. The figure below shows the plan view of the prepared sample.

Figure 10: Top view of the prepared CdTe sample.

3.2 Threshold Switching Experiment

The prepared CdTe sample was taken to a probe station equipped with micromanipulators and pogo pins. The probe station was equipped with four micromanipulators and four pogo pins. The prepared sample was first subjected to a sharp object to create a circular scribe

as shown in the figure below. The created scribe was approximately 3.5mm. One edge of the sample was treated with a sharp object to expose the TCO.

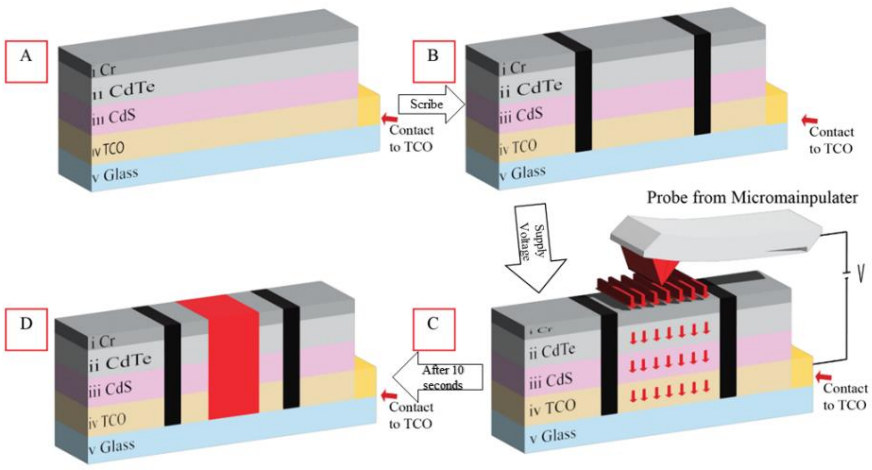

Figure 11: Cross-sectional view of the CdTe (not to scale) photovoltaics. Starting from top i) thin chromium layer ii) CdTe iii) CdS iv) glass layer (A). Cross-section of same sample after scribing (B). Red arrows indicating supply voltage to the scribe (C). Red rectangle indicating creation of a conductive shunt (D).

Two terminals of the programable DC power supply were connected to pogo pins via micromanipulators whereas, other two pogo pins were connected to a multimeter. The dc power supply was used to supply different voltage bias to the sample, while the multimeter was used to observe the resistance. The threshold switching experiment was designed to observe the resistance between the point inside the scribe and the point in the TCO. Every scribe was subjected to a different voltage bias, and an immediate change in resistance was observed. The supplied voltage ranges from -25V to +25V. Thus, 12 different scribes were created, and each scribe was provided with a different voltage. Six of the voltages were supplied with positive voltages, while the other six scribes were supplied with negative voltages. The experiment started by measuring the reference resistance between an

arbitrary point outside the scribe and TCO, Resistance(A'-X) for scribe A, Resistance (B'-X) and others, see Figure 12. These values were recorded to compare the resistance before and after the voltage bias. Also, resistance between the point inside the scribe and TCO was recorded prior to supply voltage. Scribes A, B, C, D, E, and F were supplied with 0V, 5V, 10V, 15V, 20V, and 25V for 10 seconds respectively. Similarly, scribes G, H, I, J, K, and L were supplied with 0V, -5V, -10V, -15V, -20V and -25V for 10 seconds respectively. The supplied voltage was in between the point inside the scribe and point in the TCO. The voltage supplied for scribe A was V(A-X), similarly V(B-X) for scribe B. Refer to Figure 12 (A) for schematic. After supplying voltages for 10 seconds, the voltage source was disconnected, and the multimeter was immediately connected to observe the change in resistance.

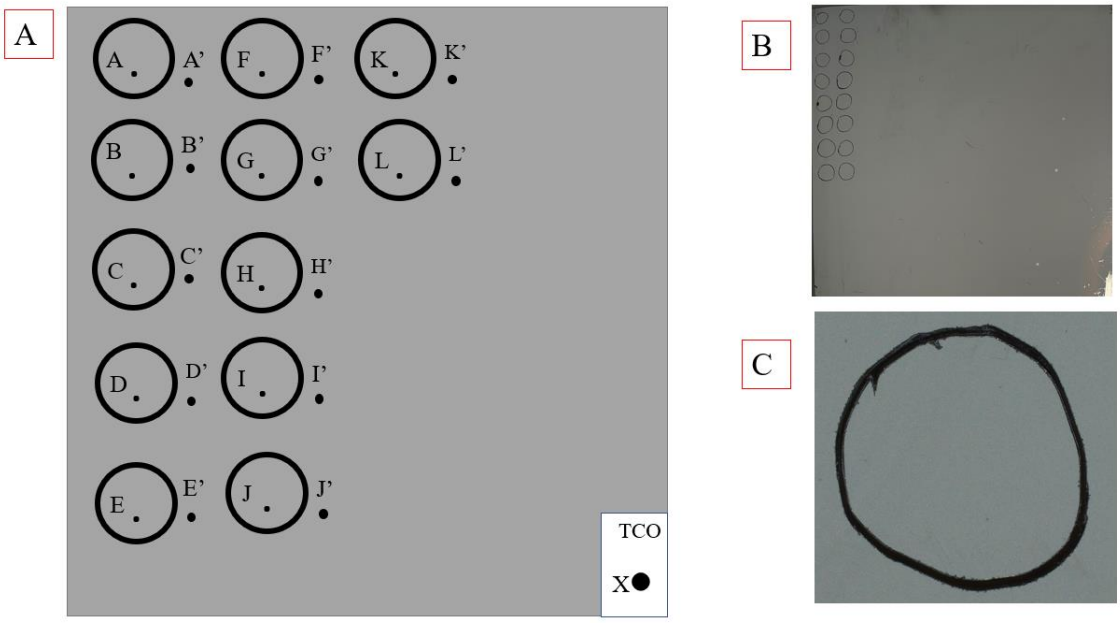

Figure 12: Schematic of the CdTe PV, point (A-L) are the points inside different scribes; point X is the point on TCO (A). Sample used for threshold switching experiment (B). Magnified image of a Scribe created on the sample (C).

3.3 Time-lapse study of switched resistance

The time-lapse study is the experiment done immediately after the completion of the threshold switching experiment. The intent is to observe a change in resistance over a period. After the threshold switching experiment, the resistance value from each scribe was recorded with the time interval of 6, 12, 24, and 48 hours. The experiment was conducted to understand the reliability of the threshold switching and endurance of its trait over time. On every time interval resistance between TCO and point inside the scribe was recorded. Figure 13 shows the experimental setup where the experiment was performed.

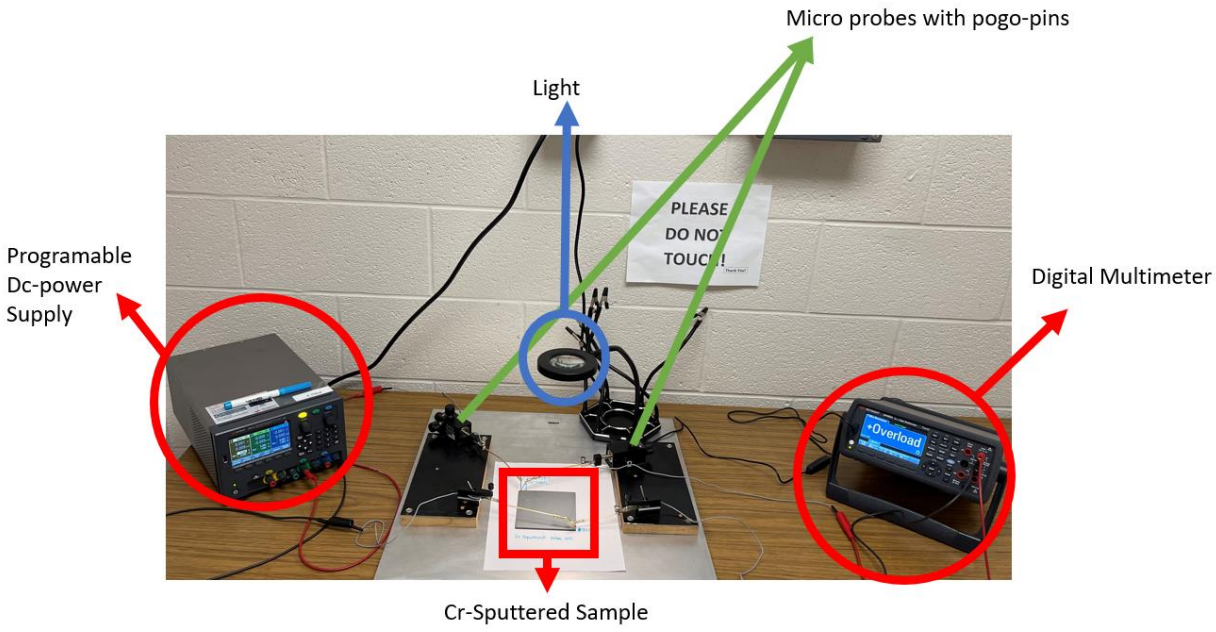

Figure 13: Experimental setup of threshold switching and time lapse study.

3.4 Circular Chromium (Cr) deposition

Cr dots were deposited on CdTe solar cell samples by RF magnetron sputtering using a Torr International sputtering system. The pressure in the deposition chamber was pumped down to below 10^{-6} Torr before the sputtering process began. The pumping system consists of a turbomolecular pump and an oil-free mechanical pump. A 2-inch 99.99% pure chromium disc target (from MSE Supplies®) was used, and on a revolving substrate holder, the solar cell sample was mounted about 15 cm above the target surface. Before starting the process, the chamber was purged with ultra-high purity grade Argon gas (Airgas, 99.9997%) for 5 minutes. Furthermore, the target was pre-sputtered for 10 minutes at a power level of 80 W in the same Ar. After that, Cr dots were deposited in the Ar environment at 70 Standard Cubic Centimeters per Minute (SCCM) flow.

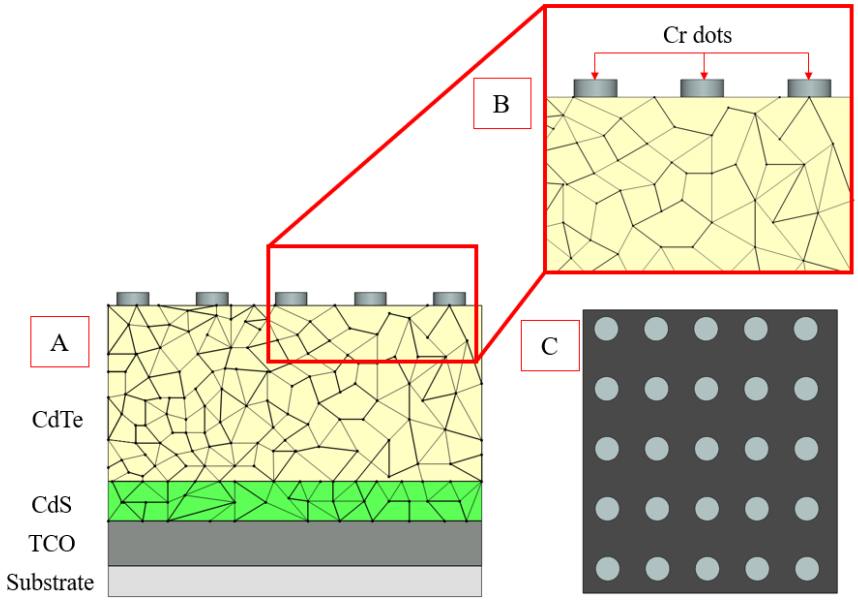

Figure 14: Schematic of CdTe PV with Circular Cr dots(A). Magnified part of Figure A, showing circular Cr dots, black line represents the granular structure. Schematic of Cr dots deposited on CdTe PV.

The deposition pressure of the chamber was at 11.5 mTorr and the chamber was at room temperature of 22 °C. The deposition time was varied from 30 seconds, 3 minutes, 6 minutes, and 10 minutes. The calibration of the thickness was done using Auger Spectroscopy. Before doing the Cr dot deposition at Solar cell sample, the continuity of the film was evaluated. Figure 14 represents the schematic of CdTe PV cell with Cr dots deposited on top whereas Figure 15 shows the magnified image of the sample taken after deposition of circular Cr spots. The grid lines on CdTe and CdS layer of Figure 14 represents the granular structure of the sample.

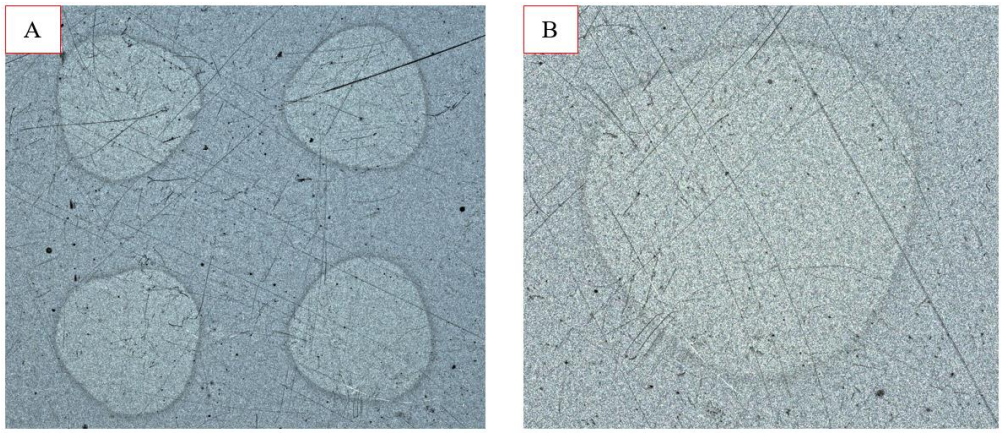

Figure :15 Circular Cr deposited on CdTe sample (A). 33x Magnified circular Cr (B).

3.5 Material characterization

3.5.1 Scanning Electron Microscopy, Focal Ion Beam, and Transmission Electron Microscopy (TEM)

The CdTe PV sample used for performing threshold switching experiment and time-lapse experiment was broken into smaller shapes, using a diamond cutter. The SEM machine sample holder had specific requirements for the dimension of the sample to be placed. The maximum acceptable dimension was 75mm in diameter and 30mm in height. Any sample less than the specified dimension could easily fit into the sample holder. The sample prepared in our case has dimensions less than the maximum specification. The sample was mounted on the sample holder using carbon tape. Copper tape was used to create a conductive path for electrons to the sample holder, which is made of aluminum. Figure 16 shows a small piece of CdTe PV cell mounted on a SEM sample holder and Scanning Electron Microscope.

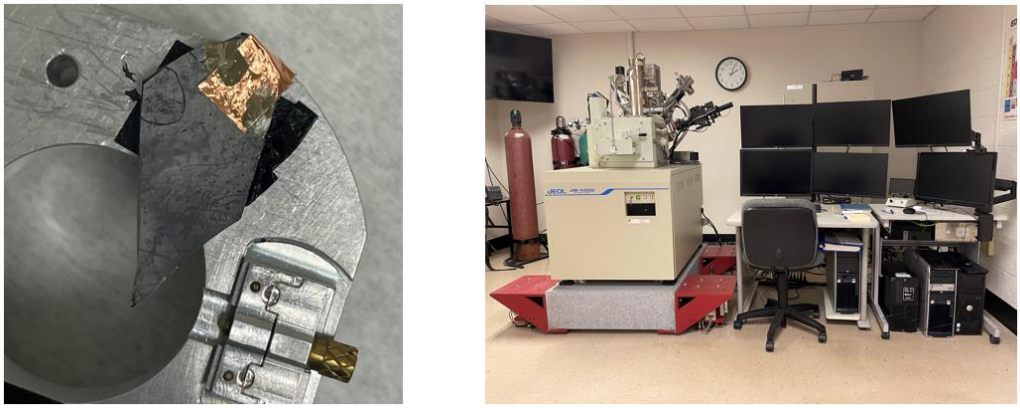

Figure 16: Sample Prepared for SEM analysis (left). SEM/FIB equipment in Electron Microscopy lab used for SEM analysis (right).

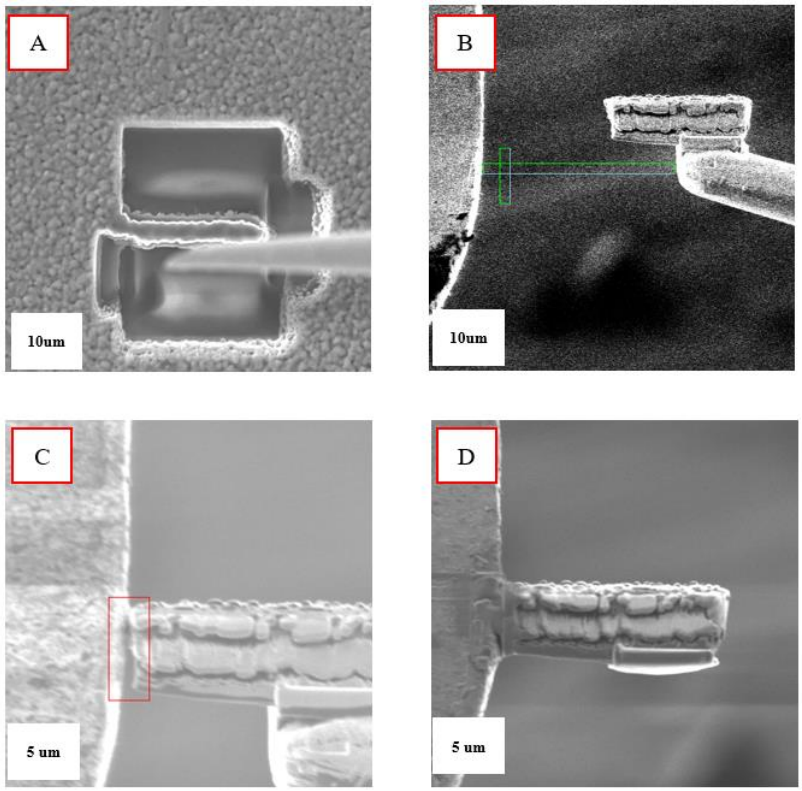

Figure 17: Steps involved in preparing TEM sample. Deposition of protective layer after milling using FIB (A). Needle soldered to the sample to weld it in a TEM sample holder (B-C), Sample after being welded in TEM holder (D).

The main objective of material characterization on this study is to analyze the layers of the PV sample used. Since we are dealing with thin film here, SEM equipment was used to perform FIB and create a sample for TEM. The sample for TEM was prepared by cutting the SEM sample using focal ion beam. First, the desired location on the sample was determined and the axis alignment was done to get the same picture on both SEM and FIB screen. The process of milling was carried out using ion beams. Once the milling was done on every side, the island structure on the middle was deposited with carbon/tungsten on top, a tungsten needle was then used to weld on the top of carbon/tungsten. Figure 17 shows

the SEM image taken during the different steps while preparing sample for TEM, using SEM-FIB technique.

The bottom layer of the specimen was cut after rotating the sample by 90^{o}. Once the specimen was ejected from the sample it was welded back to the TEM grid. The specimen was further treated with FIB to reduce the thickness and smoothen the surface with lower intensity beams. Several different intensities ion beams were used to make the specimen thinner and smoother. There were two different samples for TEM created. Figure 17 (C) and (D) shows the TEM sample grid where our created TEM sample was welded.

After multiple attempts, with several unsuccessful results, two TEM samples were prepared using SEM-FIB techniques. Both samples were handled carefully. Suction created using vacuum, was used to lift the TEM grid to install on the TEM sample holder. Which was staged into TEM for further characterization where the thickness of different layers was determined.

3.5.2 Electron Dispersive Spectroscopy (EDS)

The SEM sample, which was used to perform SEM-FIB, was also subjected to EDS analysis to confirm the back contact deposited; and to confirm the window layer of the sample. The final sample prepared for TEM was used to perform several line scans to map the elements that were deposited. Different points and lines of different widths were used to perform several scans to confirm the pattern of the elements, and their mapping on the sample. Figure 16 (left) represents the sample where EDS was performed to determine the elemental content of the back contact and window layer of the sample. While Figure 18 is

the image of the TEM sample where multiple line scans were performed to analyze the mapping of the elements on the sample.

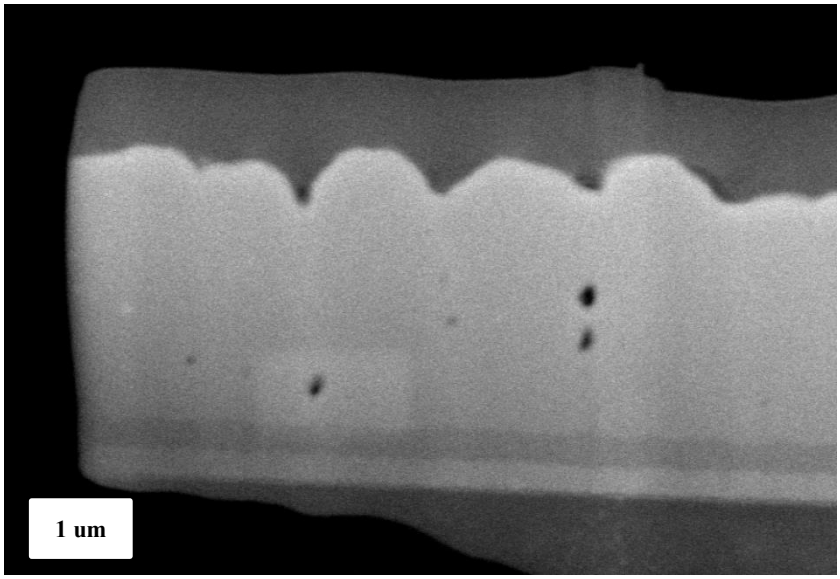

Figure 18: TEM sample used to perform EDS analysis and Line Scans.

3.5.3 Auger Electron Spectroscopy (AES)

For Auger Electron Spectroscopy analysis, samples were attached to a stainless-steel specimen holder using stainless steel screws. The holder was then inserted into the analysis chamber of a Model 660 scanning Auger surface analysis system manufactured by Physical Electronics USA of Chanhassen, MN. The chamber was evacuated to a base pressure of $\approx 2 \times 10^{-8}$ torr. A cylindrical mirror electron energy analyzer was used for electron detection. General survey spectra were collected at the surface levels and following depth profiles. Concentration vs. depth profiles were collected to show changes in elemental composition as a function of depth. Etching was accomplished using an Ar^{+} ion beam with an energy of 4keV.

CHAPTER IV

4. Results

In this chapter, the results from the experiments to verify threshold switching is presented. All the results from different experiments mentioned previously in Chapter 3 are organized here. Section 4.1 shows the results from threshold switching experiment, followed by time-lapse study of switched resistance in Section 4.2. This chapter further includes the results from the characterization techniques and concludes with the results from the experiment conducted on Circular Cr dots.

4.1 Threshold Switching

The CdTe sample, which was studied, demonstrated a rapid decrease in resistance ranging from the Mega-ohm to Kilo-ohm range when induced with both positive and negative voltage bias. The resistance values observed and recorded have been tabulated and represented in the graph below, as shown in Figure 19. This rapid decrease in resistance post voltage bias, implies that there has been a conductive path created through the point inside the scribe and TCO of the sample, which allows the electrode from the back contact to routinely contact the TCO, which is acting as a front contact for the photovoltaics cell. Table I and II below demonstrates the resistance values recorded during the threshold switching experiment, before and after supplying negative and positive voltages.

TABLE I. Change in resistance after positive voltage supply.

Scribe	Resistance across scribe and TCO prior bias	Supply Voltage(V)	Resistance across scribe and TCO after bias
A	1.07E+06 Ω	0	1.06E+06 Ω
B	1.02E+06 Ω	5	1.13E+05 Ω
C	1.05E+06 Ω	10	4.92E+04 Ω
D	1.00E+06 Ω	15	3.49E+03 Ω
E	1.01E+06 Ω	20	1.42E+04 Ω
F	1.02E+06 Ω	25	1.62E+04 Ω

TABLE II. Change in resistance after negative voltage supply.

Scribe	Resistance across scribe and TCO prior bias	Supply Voltage(V)	Resistance across scribe and TCO after bias
F	1.02E+06 Ω	0	1.02E+06 Ω
G	1.77E+06 Ω	-5	1.10E+05 Ω
H	1.08E+06 Ω	-10	1.10E+05 Ω
I	1.07E+06 Ω	-15	1.09E+05 Ω
J	1.01E+06 Ω	-20	1.63E+03 Ω
K	1.02E+06 Ω	-25	3.00E+03 Ω

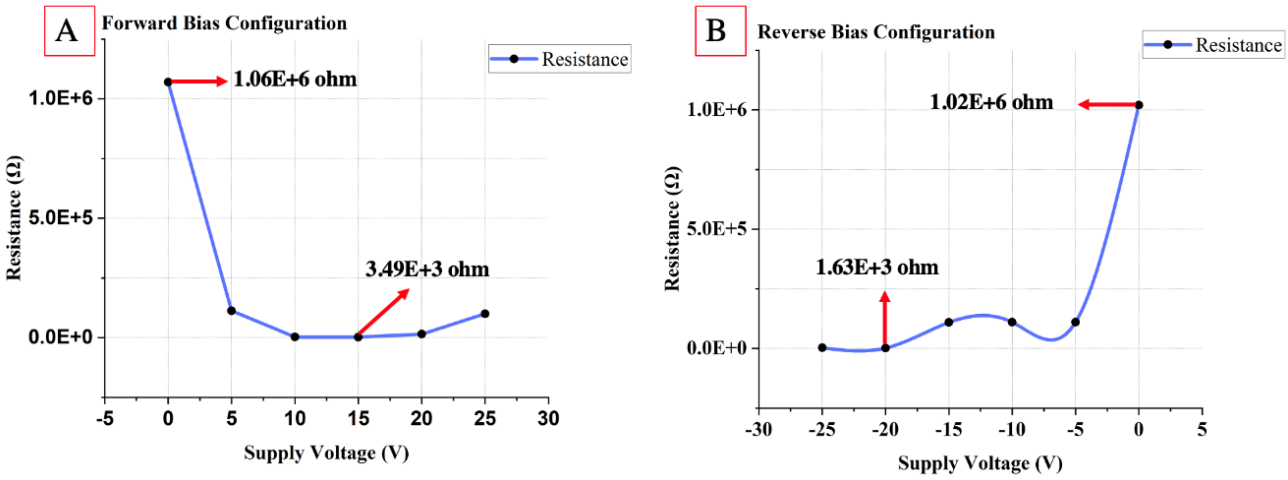

Figure 19: Rapid drop in resistance value with positive voltage bias configuration (A) and negative voltage bias configuration (B).

4.2 Time-lapse study of switched resistance

To check the reliability of the confirmed conductive shunt, a time lapse study was performed that indicated the conductive path is reliable, with a change in resistance value of about 2-KΩ. Each scribe was subjected to this experiment. We found similar results for all the scribes. Some data is tabulated and represented in the Table III below. Figure 20 represents the graphical presentation of resistance value over a period.

TABLE III. Resistance value over period

Scribe	6 hours	12 hours	24 hours	48 hours
C	2.80E+03 Ω	4.08E+03 Ω	3.39E+03 Ω	3.07E+03 Ω
D	2.06E+03 Ω	4.20E+03 Ω	3.39E+03 Ω	3.11E+03 Ω
I	4.80E+04 Ω	5.11E+04 Ω	5.10E+03 Ω	5.07E+04 Ω
K	1.96E+03 Ω	2.80E+03 Ω	2.94E+03 Ω	2.07E+03 Ω

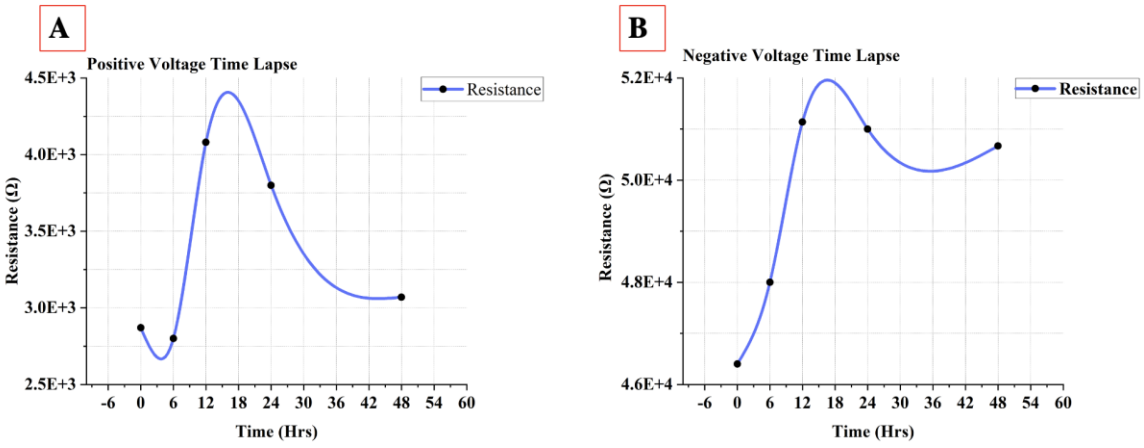

Figure 20: CdTe PV change in resistance is consistent over a period. Change in resistance where supply voltage was 10V (A) and change in resistance where supply voltage was -10V (B).

4.3 I-V Characteristic Curve Analysis in CdTe

The I-V characteristic curve is an essential tool to design circuits. Based on the function, it assists in setting voltages and current in a circuit for their proper function. So, to know the initial overall I-V characteristic of our sample, we performed a characteristic curve experiment of our sample across Cr, used as a back contact, and TCO, used as a front electrode. A non-ohmic curve was observed in the sample where the current increased with an increased in voltage, then became linear, which again increased as the voltage increased. This suggests that our sample may be considered as a non-ohmic conductor. Figure 21 shows the overall I-V characteristics of the sample across Cr and TCO.

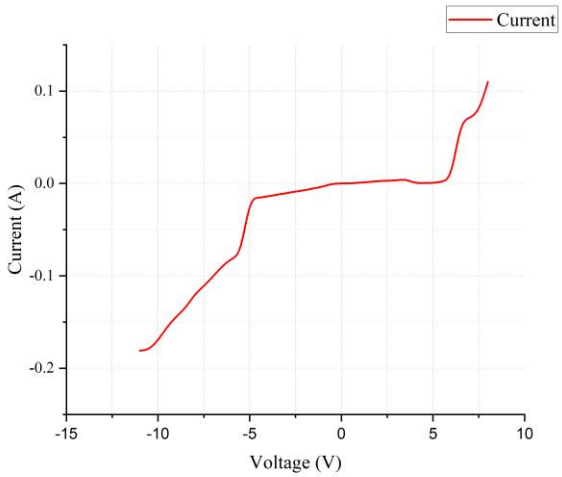

Figure 21: I-V characteristics curve of the CdTe PV across Cr and TCO.

Then, to know whether we can observe a threshold switching effect on our sample at any voltage, one point on the sample was taken where voltage was supplied with an increment of 0.5 V and the current was recorded. The results were presented as an I-V characteristic curve in Figure 22. We observe a drastic increase in current after 6V, suggesting that the

threshold switching phenomenon occurred at that voltage. To further validate our claim, we measured the same parameters on the same point of sample in the time interval of 2, 4, 6, 12, and 24 hours. We observed a linear characteristic curve. We suspect that the threshold switching effect must have occurred in 6V initially and there may be a conductive path created which led to the ohmic curve observed. This suggests that after threshold switching effect, that point in our sample behaves as an ohmic conductor.

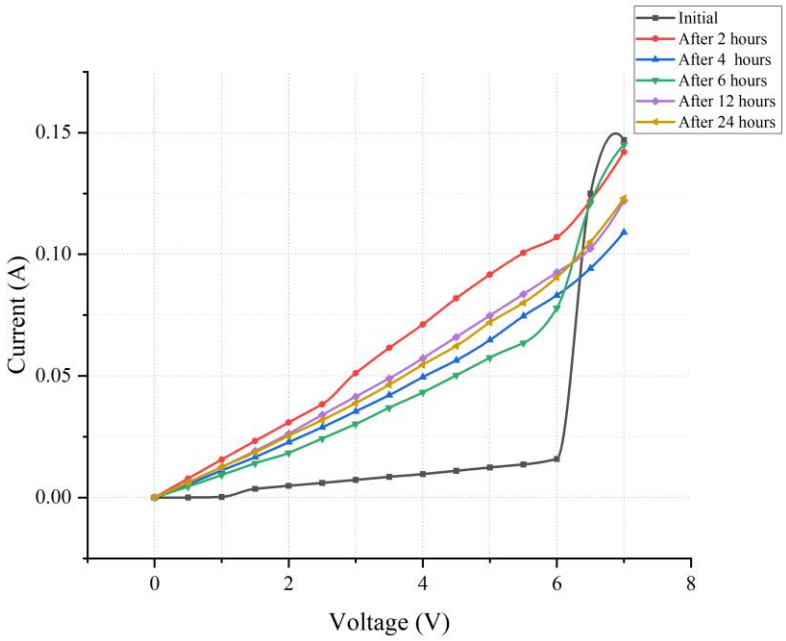

Figure 22: Characteristic curve over a period, changes to linear after formation of a conductive path.

4.4 Material Characterization of CdTe

4.4.1 EDS characterization

As we observed threshold switching phenomenon in our sample, using different experimental techniques, we then wanted to perform material characterization of our samples to know in detail which components are in them. First, we performed elemental analysis to determine the elemental composition of the sample and map the lateral distribution of the elements from the image. With the elemental analysis done using EDS, the following peaks and quant results were obtained, which are displayed in Figure 23. The result from EDS clearly shows peaks of Cadmium (Cd) and Telluride (Te), as well as Chromium (Cr) indicating the presence of CdTe, and Cr, used as a back contact, for the PV sample used.

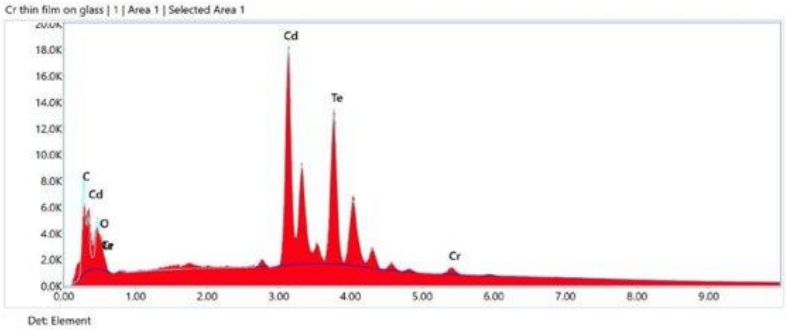

eZAF Quant Result - Analysis Uncertainty: 5.23 %

Element	Weight %	MDL	Atomic %	Net Int.	Error %	R	A	F
C K	12.7	0.14	53.8	673.9	8.9	0.7308	0.2908	1.0000
O K	3.1	0.18	9.7	205.9	11.7	0.7462	0.1477	1.0000
Cr K	1.4	0.24	1.4	115.7	15.5	0.8586	0.8521	1.0372
Cd L	39.3	0.26	17.7	2991.4	3.4	0.8211	0.8669	1.0116
Te L	43.5	0.53	17.3	2139.8	4.3	0.8351	0.8164	1.0052

Figure 23: EDS results determining Cr used as a back contact and CdTe used as absorber.

The TEM sample created using SEM-FIB technique was also used to perform elemental line scan to map the elements associated with the image. Different line scans of different

line widths and points were performed, and a graph is overlayed on top of the generated image, shown in Figure 24(B). Figure 24 shows the elemental profile plot, representing the elements determined using EDS displayed on top of the sample image.

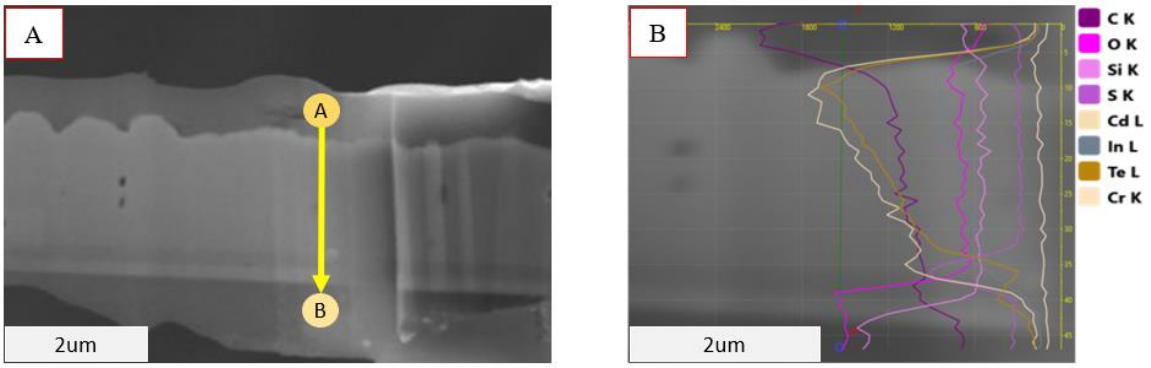

Figure 24: TEM sample representing two circular points A and B where line scan was conducted (A). Elemental profile plot showing elements concentration profile at predefine line from A to B (B).

The elemental profile plot on Figure 24 (B) clearly shows that the absorber layer is CdTe and the window layer for the sample used is CdS. The profile plot created on top of the image makes it even easier to determine the longest layer is CdTe and the layer followed by it is CdS. As we can see several components present, we can suggest that there is thin chromium layer present in the sample.

4.4.2 TEM characterization

After initial characterization of our sample, we further desired a high-resolution image of the sample and a measure thickness of its layers. First, we created a TEM sample that was inserted into the TEM chamber where the Selected-Area-Diffraction pattern was observed confirming highly oriented crystalline structure on CdTe and CdS as shown in the Figure

25 (C) and (D). Figure 25 (A) shows the image of the different layers, like carbon on the top, followed by thin layer of Cr. The thickest layer shown is CdTe and the layers followed by CdTe are CdS and TCO respectively.

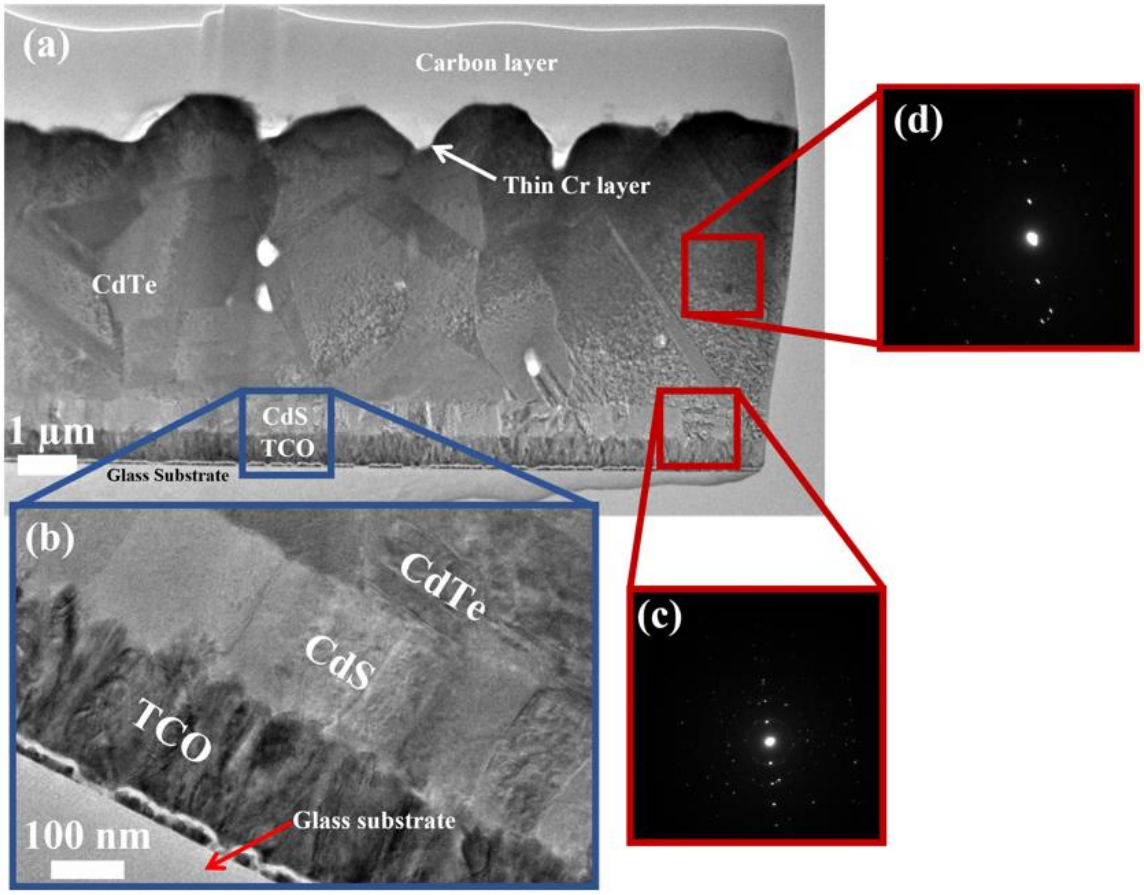

Figure 25: a) TEM image of a sample representing different layers. b) Magnified image of the n-type material followed by TCO. c) SAED pattern confirming highly oriented crystalline structure.

Furthermore, every layer in the sample was observed and Figure 26 shows the TEM image taken. This demonstrates the thickness of TCO on the top and CdS on the bottom. The length of the layers was determined using TEM measuring tool. The thickness of absorber

layer CdTe was reported to be 5um where the thickness of Window and TCO was reported to be 0.3um.

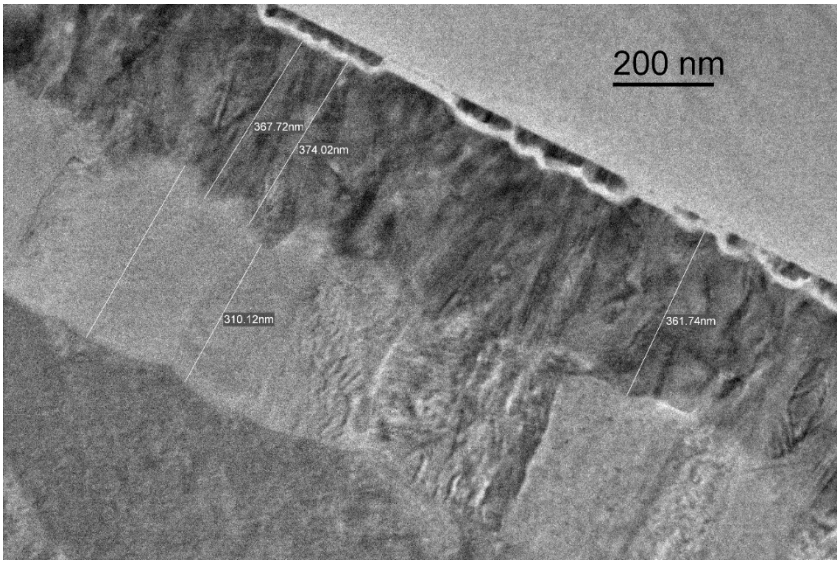

Figure 26: TEM image of the thin film measuring the thickness of TCO on top and CdS in the bottom.

4.4.3 Auger Electron Spectroscopy

To confirm the depth of Chromium layer present in our sample, we performed depth auger electron spectroscopy analysis. With the etching rate of 2nm/minute, Figure 27 shows the depth profile of the sample. Based on the half maxima of Cd and Te lines, the thickness of Cr, used as a back contact, on our sample was determined to be 13nm.

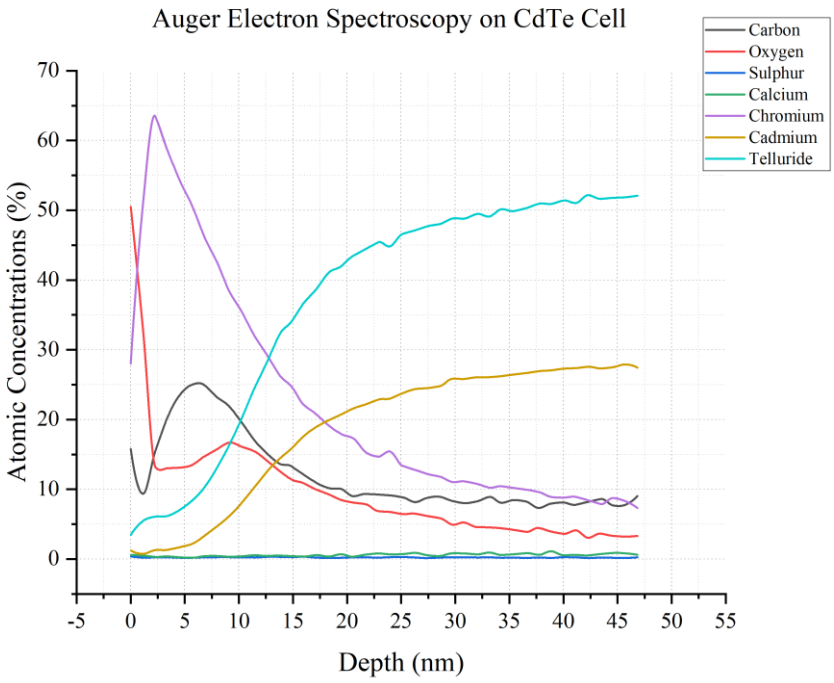

Figure 27: Auger Electron Spectroscopy depth profile for CdTe photovoltaic cell.

The AES depth profile required approximately 47 minutes to perform. The profile plot in above Figure 27 shows the presence of Carbon, Oxygen, Sulphur, Calcium, Chromium, Cadmium, and Telluride. The plot also confirms that the topmost layer is Cr, followed by a layer of CdTe. The thickness of the Cr deposited on CdTe photovoltaic cell is 13nm for the sample tested.

4.5 Circular Chromium Deposition

The intention of depositing Circular Cr is to eliminate the surface layer of back contact. After depositing the Cr on CdTe sample for 30 seconds, 3 minutes, 6 minutes, and 10 minutes, each sample was subjected to threshold switching experiment. I-V characteristics were also evaluated. The switched value of resistance was not observed in the sample where Cr dots were deposited for 30 seconds. Table IV below shows the change in resistance value observed after conducting threshold switching experiment on Cr dots deposited for 30 seconds. The value of resistance did not change from the mega ohm to kilo ohm range.

TABLE IV. Change in resistance observed after positive voltage supply on 30 seconds Cr dots.

Scribe	Resistance across scribe and TCO prior bias	Supply Voltage(V)	Resistance across scribe and TCO after bias
A	1.84E+07 Ω	0	1.14E+07 Ω
B	1.84E+07 Ω	5	1.48E+07 Ω
C	9.80E+07 Ω	10	6.90E+07 Ω
D	9.20E+07 Ω	15	2.53E+07 Ω
E	9.50E+07 Ω	20	1.57E+07 Ω
F	1.80E+07 Ω	25	2.23E+07 Ω

Therefore, further experiments were not conducted on Cr deposited for 30 seconds. The value of switched resistance observed on a sample where Cr dots were deposited for 3 minutes after performing threshold switching experiment were 55 KΩ to 65 KΩ. Which was not like what we observed in our original PV sample. Table V shows the resistance value observed during threshold switching experiment on Cr dots deposited for 3 minutes. The resistance value on Cr dots were also not in same order of magnitude prior suppling voltages. The resistance value across TCO and Scribe A, B, C were in the order of 10^6

whereas resistance value across TCO and scribe D, E, F were in the order of 10^4, 10^5, 10^2 respectively. Also, a rapid increase in current was observed after 9-10 volts in I-V characteristics analysis which is shown in Figure 28.

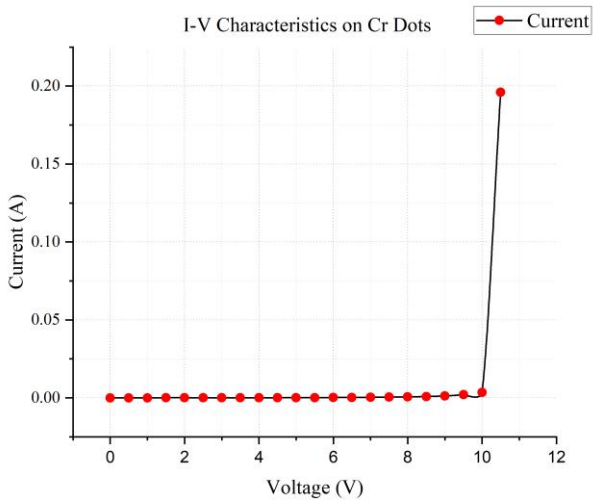

Figure 28: I-V characteristics of a Cr dots deposited for 3 minutes. Rapid increase in current was observed after 10 volts.

TABLE V. Change in resistance observed after positive voltage supply on 3minutes Cr dots.

Scribe	Resistance across scribe and TCO prior bias	Supply Voltage(V)	Resistance across scribe and TCO after bias
A	1.13E+06 Ω	0	1.13E+06 Ω
B	1.13E+06 Ω	5	1.80E+06 Ω
C	1.18E+06 Ω	10	1.05E+05 Ω
D	7.00E+04 Ω	15	5.40E+04 Ω
E	1.03E+05 Ω	20	6.50E+04 Ω
F	1.34E+02 Ω	25	5.60E+04 Ω

The sample where Cr dots were deposited for 6 minutes performed better with switched value of resistance below 20 KΩ. Table VI below shows the resistance value before and after supplying positive voltages to the sample. Also, a rapid increase in current was observed at 7 volts which is like the original sample used for this study. Figure 29 shows

the graphical representation of the switched resistance with I-V characteristics of sample for 6 minutes of Cr dots deposition.

TABLE VI. Change in resistance after positive voltage supply on Cr dots deposited for 6 minutes.

Cr dots	Resistance across scribe and TCO prior bias	Supply Voltage(V)	Resistance across scribe and TCO after bias
A	1.03E+05 Ω	0	1.03E+05 Ω
B	1.16E+05 Ω	5	1.84E+05 Ω
C	1.01E+05 Ω	10	3.12E+03 Ω
D	1.05E+05 Ω	15	1.95E+04 Ω
E	9.00E+04 Ω	20	3.60E+03 Ω
F	1.02E+05 Ω	25	4.10E+03 Ω

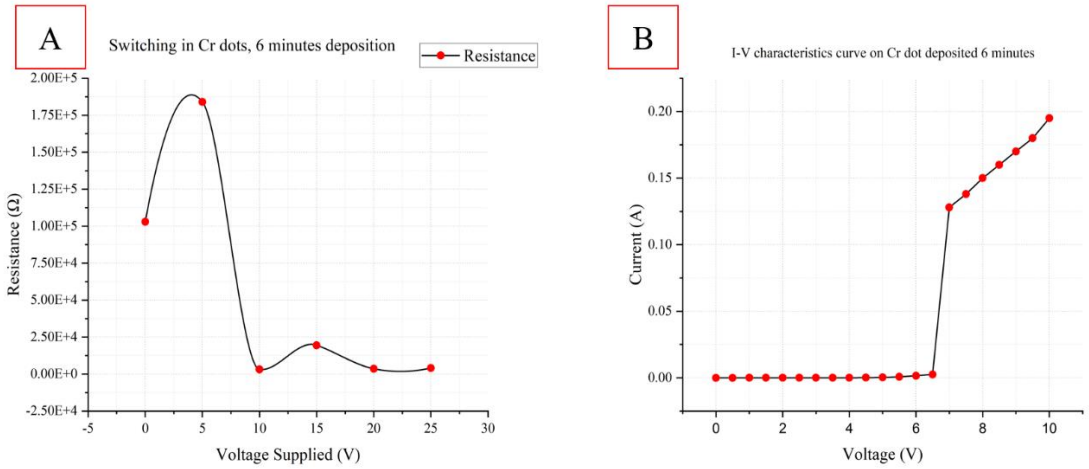

Figure 29: Rapid drop in resistance on Cr dots deposited for 6 minutes(A), I-V characteristics of the same sample (B).

Furthermore, the experimental results observed on the sample where Cr dots were deposited for 10 minutes have shown to be better, as compared to 30 seconds and 3 minutes deposition but, was not better when compared to the Cr dots deposited for 6 minutes. The switched value of resistance was under 25 k-ohms, whereas it is less than 20k-ohms for 6 minutes of deposition, and a rapid increase in current was observed after 8 volts. Figure 30

below shows the rapid drop observed, along with the I-V characteristics curve of the Cr dots with 10 minutes of deposition. Table VII shows the change in resistance value observed during threshold switching experiment conducted on Cr dots deposited for 10 minutes.

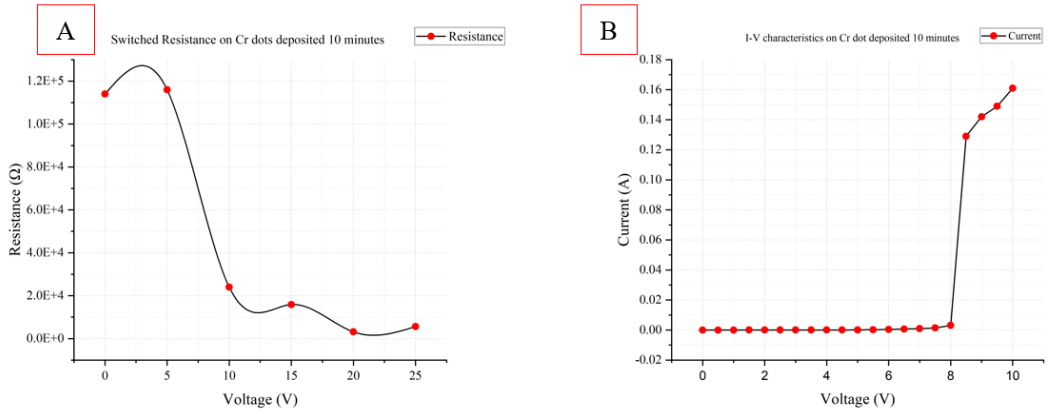

Figure 30: Rapid drop in resistance on Cr dots deposited for 10 minutes(A), I-V characteristics of the same sample (B).

Based on the results obtained by running the threshold switching experiment and I-V characteristics across Cr dots and TCO, no change in resistance value was observed after supplying voltages on the 30 seconds deposited Cr dots. Change in resistance value was observed in the 3 minutes of Cr deposition whereas, the change in order of magnitude was not significant. The Cr dots deposited for 6 minutes, and 10 minutes performed better in term of switching. However, the Cr dots deposited for 6 minutes gave better result in terms of switched resistance value and characteristic curve. Based on the results obtained, thickness of the Cr dots does play a role in achieving threshold switching in CdTe PV cell.

The thickness of the Cr dots deposited were calibrated using Auger electron spectroscopy. Table VIII shows the thickness of Cr dots deposited corresponding to the deposition time. Figure 31 shows the schematic representation of a conductive red path created after supplying different voltages across Cr-dots.

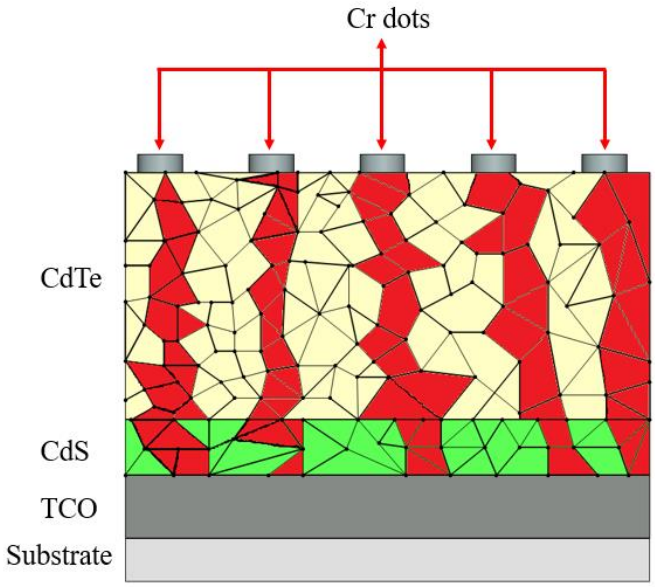

Figure 31: Representation of an electric conductive path (red grains) created after supplying voltages across Cr dots and TCO.

TABLE VIII. Thickness of Cr dots corresponding to deposition time.

S. N	Deposition Time	Deposition Technique	Deposited thickness
1	30 sec	RF magnetron sputtering	1.5nm
2	2 minutes	RF magnetron sputtering	6nm
3	3 minutes	RF magnetron sputtering	9nm
4	6 minutes	RF magnetron sputtering	18nm
5	10 minutes	RF magnetron sputtering	30nm

CHAPTER V

5. Conclusion

In this thesis, the experimental verification of threshold switching in CdTe photovoltaics was studied. Several studies have discussed threshold switching phenomena and materials that demonstrate these phenomena [40]. Here, we experimentally verify this phenomenon in CdTe cells which may be potentially incorporated into the PV manufacturing for improving the manufacturing efficiency of the thin-film PVs.

Our experimental results imply that the voltage bias creates a conductive filament from the topmost layer through the PV stack to the buried electrode, through the phenomenon of threshold switching. Time lapse study of the conductive filament's resistance suggests that the threshold switching phenomenon is reliable, as the switched resistance did not change after 48 hours. This novel method could potentially lead to scribe-less manufacturing technology of PVs, by eliminating the back contact. Switching was observed on both positive and negative voltage configuration and the switching effect lasted longer, implying its reliability.

Moreover, the IV characteristics of the CdTe sample was successfully performed. The initial IV curve was non-linear and demonstrated a non-ohmic curve with increasing voltage values. However, when the supplied voltage to a particular point in the sample crosses 6 V, we saw a rapid increase in the current, indicating the occurrence of threshold switching phenomena around 6V. After observing the threshold switching, the I-V characteristics on the same point of the sample were observed to be linear i.e., ohmic in

nature, suggesting that the threshold switching phenomenon , a results in a creation of a conducting filament.

We also characterized our sample to using SEM, FIB, TEM, EDS, and AES. EDS detected the layer of chromium layer, as well as several other layers of materials present. Furthermore, TEM investigation enables us to detect layers of TCO, CdS and CdTe with thicknesses of 0.3 um, 0.3 um and 5 um respectively. AES further shows the thickness of Cr to be 13nm, which confirms the presence of Cr in the sample.

Deposition of Cr dots of different thickness gave us insight about how the thickness is important to achieve the threshold switching phenomenon. With varying thicknesses of Cr dots deposited, better results in term of switched resistance and I-V characteristics were only observed on the Cr dot with the thickness of 18 nm.

Overall, this study experimentally verifies the threshold switching effect in CdTe cells, which was shown by a drastic decrease in resistance and an increase in current after a certain threshold voltage value is achieved. The conventional laser scribing technology is costly and unreliable. However, this study showed that the threshold switching technique is reliable as shown by the time lapse study conducted. In a nutshell, threshold switching was experimentally verified in CdTe cells, and this phenomenon could potentially lead to scribe-less technology, by eliminating the conventional tedious and expensive laser scribing.

References

[1] M. H. Shubbak, "Advances in solar photovoltaics: Technology review and patent trends," *Renewable and Sustainable Energy Reviews*, vol. 115. Elsevier Ltd, Nov. 01, 2019. doi: 10.1016/j.rser.2019.109383.

[2] D. D. B. Mesquita, J. Lucas, S. Silva, H. S. Moreira, M. Kitayama, and M. G. Villalva, "A review and analysis of technologies applied in PV modules."

[3] A. Bosio, A. Romeo, D. Menossi, S. Mazzamuto, and N. Romeo, "Review: The second-generation of CdTe and CuInGaSe2 thin film PV modules," in *Crystal Research and Technology*, Aug. 2011, pp. 857–864. doi: 10.1002/crat.201000586.

[4] T. Saga, "Advances in crystalline silicon solar cell technology for industrial mass production," *NPG Asia Materials*, vol. 2, no. 3. pp. 96–102, Jul. 2010. doi: 10.1038/asiamat.2010.82.

[5] M. T. Zarmai, N. N. Ekere, C. F. Oduoza, and E. H. Amalu, "A review of interconnection technologies for improved crystalline silicon solar cell photovoltaic module assembly," *Applied Energy*, vol. 154. Elsevier Ltd, pp. 173–182, Sep. 15, 2015. doi: 10.1016/j.apenergy.2015.04.120.

[6] R. W. Miles, "Photovoltaic solar cells: Choice of materials and production methods," *Vacuum*, vol. 80, no. 10, pp. 1090–1097, Aug. 2006, doi: 10.1016/j.vacuum.2006.01.006.

[7] J. Jeong, N. Park, W. Hong, and C. Han, "Analysis for the degradation mechanism of photovoltaic ribbon wire under thermal cycling," in *2011 37th IEEE Photovoltaic Specialists Conference*, 2011, pp. 3159–3161. doi: 10.1109/PVSC.2011.6186611.

[8] V. v. Tyagi, N. A. A. Rahim, N. A. Rahim, and J. A. L. Selvaraj, "Progress in solar PV technology: Research and achievement," *Renewable and Sustainable Energy Reviews*, vol. 20. Elsevier Ltd, pp. 443–461, 2013. doi: 10.1016/j.rser.2012.09.028.

[9] V. Fthenakis, "Sustainability of photovoltaics: The case for thin-film solar cells," *Renewable and Sustainable Energy Reviews*, vol. 13, no. 9. pp. 2746–2750, Dec. 2009. doi: 10.1016/j.rser.2009.05.001.

[10] A. G. Aberle, "Thin-film solar cells," *Thin Solid Films*, vol. 517, no. 17, pp. 4706–4710, Jul. 2009, doi: 10.1016/j.tsf.2009.03.056.

[11] H. Booth, "Laser processing in industrial solar module manufacturing," *Journal of Laser Micro Nanoengineering*, vol. 5, no. 3, pp. 183–191, Dec. 2010, doi: 10.2961/jlmn.2010.03.0001.

[12] V. G. Karpov, D. Shvydka, and S. S. Bista, "Threshold switching in solar cells and a no-scribe photovoltaic technology," *Appl Phys Lett*, vol. 119, no. 19, Nov. 2021, doi: 10.1063/5.0066434.

[13] T. J. McMahon, “Accelerated testing and failure of thin-film PV modules,” *Progress in Photovoltaics: Research and Applications*, vol. 12, no. 2–3, pp. 235–248, 2004, doi: 10.1002/pip.526.
[14] W. Kriihler, “Amorphous Thin-Film Solar Cells*,” 1991.
[15] S. Cao *et al.*, “Light Propagation in Flexible Thin-Film Amorphous Silicon Solar Cells with Nanotextured Metal Back Reflectors,” *ACS Appl Mater Interfaces*, vol. 12, no. 23, pp. 26184–26192, Jun. 2020, doi: 10.1021/acsami.0c05330.
[16] R. Noufi and K. Zweibel, “High-Efficiency CdTe and CIGS Thin-Film Solar Cells: Highlights and Challenges; Preprint,” 2006. [Online]. Available: http://www.osti.gov/bridge
[17] M. W. Bouabdelli, F. Rogti, M. Maache, and A. Rabehi, “Performance enhancement of CIGS thin-film solar cell,” *Optik (Stuttg)*, vol. 216, Aug. 2020, doi: 10.1016/j.ijleo.2020.164948.
[18] D. Bonnet, “The CdTe thin film solar cell - an overview,” *International Journal of Solar Energy*, vol. 12, no. 1–4, pp. 1–14, 1992, doi: 10.1080/01425919208909746.
[19] I. M. Dharmadasa, “Review of the CdCl 2 treatment used in CdS/CdTe thin film solar cell development and new evidence towards improved understanding,” *Coatings*, vol. 4, no. 2. MDPI AG, pp. 282–307, Jun. 01, 2014. doi: 10.3390/coatings4020282.
[20] X. Wu and P. Sheldon, “Novel CdTe Cell Fabrication Process with Potential for Low Cost and High Throughput,” 2000.
[21] J. E. Greene, “Review Article: Tracing the recorded history of thin-film sputter deposition: From the 1800s to 2017,” *Journal of Vacuum Science & Technology A: Vacuum, Surfaces, and Films*, vol. 35, no. 5, p. 05C204, Sep. 2017, doi: 10.1116/1.4998940.
[22] M. S. Raven, “Review Radio frequency sputtering and the deposition of high-temperature superconductors,” 1994.
[23] I. Repins *et al.*, “19.9%-efficient ZnO/CdS/CuInGaSe2 solar cell with 81.2% fill factor,” *Progress in Photovoltaics: Research and Applications*, vol. 16, no. 3, pp. 235–239, May 2008, doi: 10.1002/pip.822.
[24] N. Mufti *et al.*, “Review of CIGS-based solar cells manufacturing by structural engineering,” *Solar Energy*, vol. 207. Elsevier Ltd, pp. 1146–1157, Sep. 01, 2020. doi: 10.1016/j.solener.2020.07.065.
[25] X. He *et al.*, “The role of oxygen doping on elemental intermixing at the PVD-CdS/Cu (InGa)Se 2 heterojunction,” *Progress in Photovoltaics: Research and Applications*, vol. 27, no. 3, pp. 255–263, Mar. 2019, doi: 10.1002/pip.3087.
[26] M. G. Tsai *et al.*, “Annealing effect on the properties of Cu(In0.7Ga 0.3)Se2 thin films grown by femtosecond pulsed laser deposition,” *Journal of the American Ceramic Society*, vol. 96, no. 8, pp. 2419–2423, Aug. 2013, doi: 10.1111/jace.12422.
[27] J. H. Park *et al.*, “The deposition of thin films of CuME2 by CVD techniques (M = In, Ga and E = S, Se),” *J Mater Chem*, vol. 13, no. 8, pp. 1942–1949, Aug. 2003, doi: 10.1039/b302896h.

[28] M. Venkatachalam, M. D. Kannan, S. Jayakumar, R. Balasundaraprabhu, and N. Muthukumarasamy, “Effect of annealing on the structural properties of electron beam deposited CIGS thin films,” *Thin Solid Films*, vol. 516, no. 20, pp. 6848–6852, Aug. 2008, doi: 10.1016/j.tsf.2007.12.127.
[29] T. Nakada, K. Furumi, and A. Kunioka, “High-Efficiency Cadmium-Free Cu(In,Ga)Se Thin-Film Solar Cells with Chemically Deposited ZnS Buffer Layers,” 1999.
[30] G. Fang, D. Li, and B.-L. Yao, “Fabrication and vacuum annealing of transparent conductive AZO thin films prepared by DC magnetron sputtering,” 2003.
[31] P. Gečys *et al.*, “CIGS thin-film solar module processing: Case of high-speed laser scribing,” *Sci Rep*, vol. 7, Jan. 2017, doi: 10.1038/srep40502.
[32] D. Shvydka, V. G. Karpov, and A. D. Compaan, “Bias-dependent photoluminescence in CdTe photovoltaics,” *Appl Phys Lett*, vol. 80, no. 17, pp. 3114–3116, Apr. 2002, doi: 10.1063/1.1475359.
[33] D. L. Bätzner, A. Romeo, M. Terheggen, M. Döbeli, H. Zogg, and A. N. Tiwari, “Stability aspects in CdTe/CdS solar cells,” in *Thin Solid Films*, Mar. 2004, pp. 536–543. doi: 10.1016/j.tsf.2003.10.141.
[34] IEEE Electron Devices Society, Annual IEEE Computer Conference, Fla. IEEE Photovoltaic Specialists Conference 39 2013.06.16-21 Tampa, Fla. PVSC 39 2013.06.16-21 Tampa, and Fla. IEEE PV Specialists Conference 39 2013.06.16-21 Tampa, *2013 IEEE 39th Photovoltaic Specialists Conference (PVSC) 16-21 June 2013, Tampa, Florida*.
[35] G. Altamura *et al.*, “Alternative back contacts in kesterite Cu2ZnSn(S 1-xSex)4 thin film solar cells,” in *Journal of Renewable and Sustainable Energy*, American Institute of Physics Inc., Jan. 2014. doi: 10.1063/1.4831781.
[36] IEEE Electron Devices Society, Annual IEEE Computer Conference, Fla. IEEE Photovoltaic Specialists Conference 39 2013.06.16-21 Tampa, Fla. PVSC 39 2013.06.16-21 Tampa, and Fla. IEEE PV Specialists Conference 39 2013.06.16-21 Tampa, *2013 IEEE 39th Photovoltaic Specialists Conference (PVSC) 16-21 June 2013, Tampa, Florida*.
[37] J. Zhang, R. Kondrotas, S. Lu, C. Wang, C. Chen, and J. Tang, “Alternative back contacts for Sb2Se3 solar cells,” *Solar Energy*, vol. 182, pp. 96–101, Apr. 2019, doi: 10.1016/j.solener.2019.02.050.
[38] S. Hudgens, “Progress in understanding the Ovshinsky Effect: Threshold switching in chalcogenide amorphous semiconductors,” *Physica Status Solidi (B) Basic Research*, vol. 249, no. 10. Wiley-VCH Verlag, pp. 1951–1955, 2012. doi: 10.1002/pssb.201200420.
[39] Z. Wang *et al.*, “Resistive switching materials for information processing,” *Nature Reviews Materials*, vol. 5, no. 3. Nature Research, pp. 173–195, Mar. 01, 2020. doi: 10.1038/s41578-019-0159-3.
[40] V. G. Karpov, D. Shvydka, and S. S. Bista, “Threshold switching in solar cells and a no-scribe photovoltaic technology,” *Appl Phys Lett*, vol. 119, no. 19, Nov. 2021, doi: 10.1063/5.0066434.

[41] S. Devkota *et al.*, “Threshold Switching in CdTe Photovoltaics,” *ECS Trans*, vol. 109, no. 1, pp. 3–10, Sep. 2022, doi: 10.1149/10901.0003ecst.
[42] Y. Yamaguchi *et al.*, “REVERSIBLE ELECTRICAL SWITCHING PHENOMENA IN DISORDERED STRUCTURES.pdf,” Cambridge University Press, 1960.
[43] V. G. Karpov, Y. A. Kryukov, I. v. Karpov, and M. Mitra, “Field-induced nucleation in phase change memory,” *Phys Rev B Condens Matter Mater Phys*, vol. 78, no. 5, Aug. 2008, doi: 10.1103/PhysRevB.78.052201.
[44] Z. Wang *et al.*, “Threshold Switching of Ag or Cu in Dielectrics: Materials, Mechanism, and Applications,” *Adv Funct Mater*, vol. 28, no. 6, Feb. 2018, doi: 10.1002/adfm.201704862.
[45] “SEM vs TEM.”
[46] J. S. Lee, R. T. Hill, A. Chilkoti, and W. L. Murphy, “Surface Patterning,” *Biomater Sci*, pp. 553–573, Jan. 2020, doi: 10.1016/B978-0-12-816137-1.00037-4.
[47] J. Yan and N. Takayama, “Introduction,” in *Micro and Nanoscale Laser Processing of Hard Brittle Materials*, Elsevier, 2020, pp. 1–16. doi: 10.1016/b978-0-12-816709-0.00001-x.
[48] “TEM-description”.